Cell

The Polarisome Is Required for Segregation and Retrograde Transport of Protein Aggregates

Beidong Liu,[1,*] Lisa Larsson,[1] Antonio Caballero,[1] Xinxin Hao,[1] David Öling,[1] Julie Grantham,[1] and Thomas Nyström[1,*]
[1]Department of Cell and Molecular Biology, University of Gothenburg, Medicinaregatan 9C, 413 90 Göteborg, Sweden
*Correspondence: beidong.liu@cmb.gu.se (B.L.), thomas.nystrom@cmb.gu.se (T.N.)
DOI 10.1016/j.cell.2009.12.031

SUMMARY

The paradigm sirtuin, Sir2p, of budding yeast is required for establishing cellular age asymmetry, which includes the retention of damaged and aggregated proteins in mother cells. By establishing the global genetic interaction network of *SIR2* we identified the polarisome, the formin Bni1p, and myosin motor protein Myo2p as essential components of the machinery segregating protein aggregates during mitotic cytokinesis. Moreover, we found that daughter cells can clear themselves of damage by a polarisome- and tropomyosin-dependent polarized flow of aggregates into the mother cell compartment. The role of Sir2p in cytoskeletal functions and polarity is linked to the CCT chaperonin in *sir2*Δ cells being compromised in folding actin. We discuss the findings in view of recent models hypothesizing that polarity may have evolved to avoid clonal senescence by establishing an aging (soma-like) and rejuvenated (germ-like) lineage.

INTRODUCTION

One of August Weismann's evolutionary theories of aging proposes that aging evolved in organisms that segregate germ and soma (Weismann, 1889) because such organisms must invest additional resources to reproduce instead of maintaining the soma, which, as a consequence, deteriorate and age. The quintessence of Weismann's germ plasm theory forms the platform also of the disposable soma theory of aging (Kirkwood, 1977; Kirkwood and Holliday, 1979), which predicts that (1) aging occurs due to the progressive accumulation of damage in somatic cells, (2) aging occurs due to resource limitations, the more an animal expends on germ cell quality and reproduction, the less resources are available for somatic damage protection, and (3) the optimal balance between somatic maintenance and damage protection versus reproduction is dictated by the pressures of the external environment.

Following the arguments of Weismann and contemporary evolutionary theories of aging, unicellular microorganisms displaying nonconservative dispersion of both undamaged and damaged constituents during cytokinesis may not be considered bona fide aging organisms regardless of being useful models for aging or specific aspects of the aging process. However, it has been suggested that asymmetry in simple unicellular systems might develop into aging and that sibling-specific deterioration may confer a selective advantage in unicellular organisms (Kirkwood, 1981; Partridge and Barton, 1993). Indeed, there are a growing number of examples of unicellular organisms displaying lineage-specific aging and a division of labor between the cells produced during cytokinesis (Ackermann et al., 2003; Aguilaniu et al., 2003; Barker and Walmsley, 1999; Erjavec et al., 2008; Nyström, 2007; Stewart et al., 2005). For example, the budding yeast *Saccharomyces cerevisiae* displays asymmetrical cytokinesis in which one of the siblings (the larger mother cell) undergoes age-related deterioration and with repeated divisions eventually loses the capacity to divide. Yet, the aging mother cell is capable of generating daughter cells, arguably a kind of germ cell equivalent, with a full replicative potential (Kaeberlein et al., 2007; Sinclair and Guarente, 1997). This generation of rejuvenated progeny encompasses a process limiting the inheritance of toxic and deteriorated material, including extrachromosomal rDNA circles (ERCs) (Shcheprova et al., 2008; Sinclair and Guarente, 1997) and oxidatively damaged and aggregated proteins (Aguilaniu et al., 2003; Erjavec et al., 2007; Erjavec and Nyström, 2007). Recent reports have shown that partitioning of damaged and potentially toxic protein species, known as spatial quality control (SQC), occurs also in unicellular systems dividing by binary fission, including *Escherichia coli* and *Schizosaccharomyces pombe,* and that the damage-enriched sibling lineages show signs of aging and decreased fitness (Erjavec et al., 2008; Lindner et al., 2008). Interestingly, mitotic segregation of damage and the establishment of a soma-like and germ-like lineage in both *S. pombe* and *S. cerevisiae* requires the sirtuin Sir2p (Aguilaniu et al., 2003; Erjavec et al., 2008; Erjavec and Nyström, 2007), a protein deacetylase and life-span modulator in yeast, worms, flies and fish (Guarente, 2000; Imai et al., 2000; Rogina and Helfand, 2004; Sinclair, 2002; Tissenbaum and Guarente, 2001). However, apart from the fact that Sir2p, in concert with the protein-aggregate remodeling factor Hsp104p, is required for SQC (Erjavec et al., 2007; Tessarz et al., 2009) little is known about the machineries involved in establishing asymmetrical inheritance of proteotoxic damage.

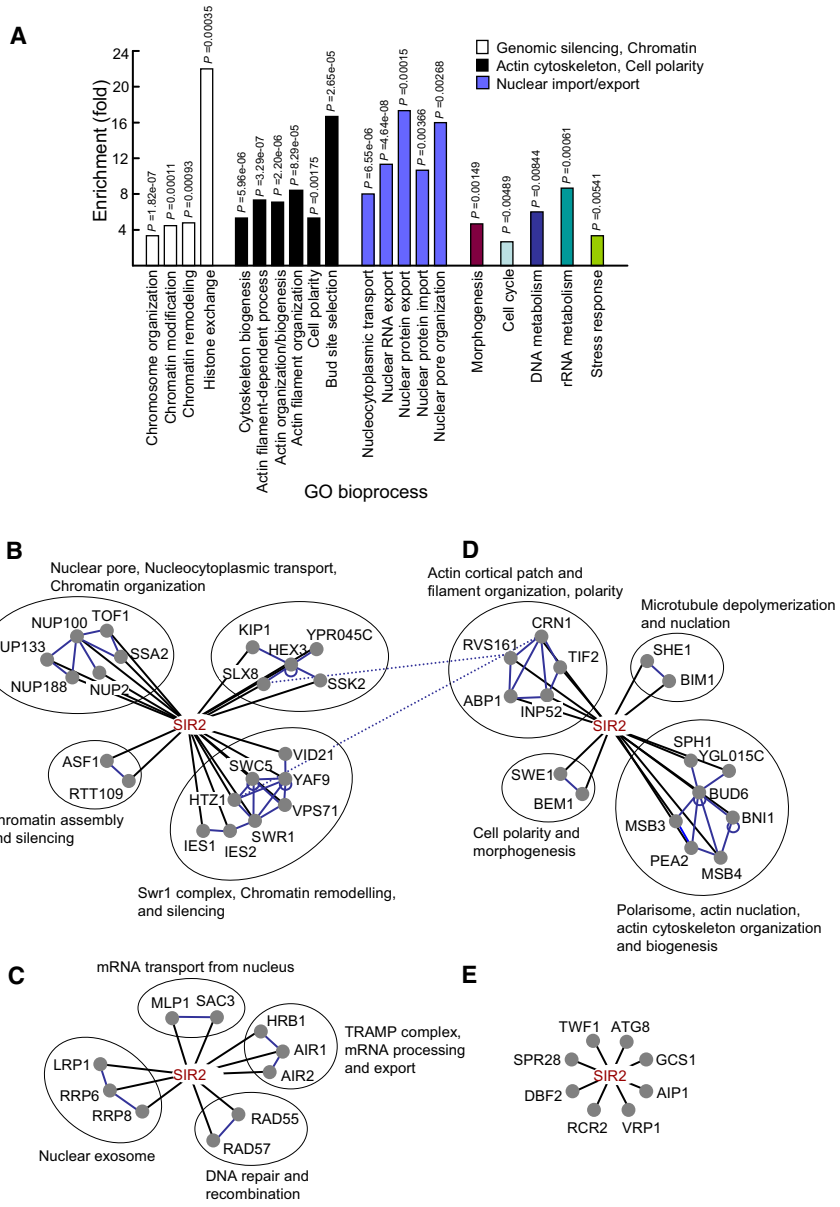

Figure 1. Functional Enrichment Analysis of the *SIR2* Genetic Interaction Network

(A) The confirmed *SIR2* SS interactions were analyzed for enrichment of gene ontology-bioprocess groups by comparison to a background list of SGA-V2 array (4261 genes) using a p value cut-off $p < 0.01$. p values were generated using a hypergeometric distribution with multiple hypothesis correction.

(B–E) Networks of protein complexes and individual genes showing SS interactions with *SIR2*. Genes showing SS interactions (nodes) were grouped in modules based on their known physical interactions (blue edges). SS interactions found in this study between *SIR2* and complexes are displayed with black edges (see also Figure S1 for construction of *sir2*Δ query strain and Table S3 for the full list of genetic interactions identified in the *SIR2* SGA screen).

Since computational modeling suggests that a failure to segregate protein damage may result in a reduced fitness (Erjavec et al., 2008) and functions crucial for cellular fitness are often performed by parallel partly redundant pathways, we hypothesized that machineries involved in the partitioning of protein aggregates could be identified by systematically screening for genetic interactions between *SIR2* and nonessential and essential genes using synthetic genetic arrays (SGA) analysis (Tong et al., 2001, 2004). Using this approach, we found that cells lacking Sir2p share many genetic interactions with the conditional actin mutant, which is a result of *sir2Δ* cells showing a defect in CCT-chaperonin-dependent folding of actin. The global genetic interaction analysis of *SIR2* also identified the polarisome as the machinery required for mitotic partitioning of protein aggregates, and we demonstrate that tropomyosin- and formin-dependent actin nucleation at the polarisome, but not the septin ring, provides the daughter cells with the means of clearing themselves of protein damage by a retrograde flow of aggregates into the progenitor cell, which effectively acts as a waste-disposal cell.

RESULTS

Global Genetic Interaction Network of *SIR2* Reveals a Role for the Sirtuin in Cellular Polarity

We first engineered a *sir2* mutant such that it could serve as a query strain proficient in all steps required for SGA double-mutant constructions. To achieve this, both the *HMR* and *HML* loci were deleted in a *sir2*Δ *MAT*α haploid background to enable mating and subsequent germination of *MAT***a** progeny, as facilitated by the SGA reporter (*can1*-Δ*::STE2pr-Sp_his5*), which is only expressed in *MAT***a** cells (Figure S1 available online).

The engineered *sir2*Δ query strain was applied to SGA analysis and 122 synthetic sick (SS) interactions were confirmed using the Bioscreen approach (Warringer et al., 2003) (Table S3). When assessing the relationship between the genetic interactions with gene ontology (GO) functional attributes we found that genetic interactions with *SIR2* were significantly enriched among genes with assignments in (1) genomic silencing and chromatin structure, (2) nuclear export/import processes, and, unexpectedly, (3) actin cytoskeleton biogenesis, organization, and function (Figure 1A). Scoring for functional relationships based on SS interactions between *SIR2* and genes encoding proteins known to interact with one another physically confirmed such a pattern—i.e., enrichment was found between *SIR2* and

genes coding for products that form complexes involved in chromatin assembly, organization, remodeling, and silencing as well as nuclear pore functions and nucleocytoplasmic transport (Figure 1B). *SIR2* also buffers against defects in nuclear RNA surveillance systems, including the nuclear exosome, the *MLP1*/*SAC3* mRNA transporter, the TRAMP complex for RNA processing and export (Figure 1C), and *RAD55*/*RAD57*-dependent repair (Figure 1C). Again, SS interactions were also markedly enriched between *SIR2* and genes encoding proteins involved in actin cytoskeleton functions, especially those required for establishing cell polarity, including several polarisome components (Figures 1D and 1E).

The polarisome is a functional complex within the polarity cap network consisting of the core proteins Bni1p, Pea2p, Bud6p, and Spa2p (Moseley and Goode, 2006). Bni1p is one of two yeast formins and a central factor of the polarisome due to its role in nucleating actin cable assembly (Pruyne et al., 2002; Sagot et al., 2002). However, a genetic interaction between *BNI1* and *SIR2* could not be screened due to the linkage effect between *BNI1* (YNL271C) and one of the anti-diploid markers *lyp1Δ* (YNL268W). Therefore, we crossed the *BNI1* mutant to the *SIR2* query strain separately and performed tetrad dissection to check the fitness of single and double mutants. In addition, a *sir2Δ bni1Δ* double mutant was also constructed by standard PCR knockout procedures and its fitness compared with that of wild-type (WT) and single mutants in liquid cultures. Both procedures demonstrated that *SIR2* and *BNI1* interact genetically and that a *sir2Δ bni1Δ* mutant displays severe fitness defects (Figures 2A and 2B). We deleted the *FOB1* gene in this genetic background (the *fob1*Δ mutation reduces ERCs to levels lower than the wild-type; Defossez et al., 1999), which demonstrated that the reduced fitness of a *sir2Δ bni1Δ* double mutant is unrelated to ERC accumulation (Figure 2B). Deleting *BNR1* and thus encoding the formin that, in contrast to Bni1p, is associated with the septin ring rather than the polarisome did not result in a fitness reduction of the *sir2* deletion mutant (not shown).

The reduced fitness of cells lacking *SIR2* and either *BUD6* or *BNI1* was accompanied by an increased sensitivity to the actin-depolarizing drug Latranculin-B (Figure 2C), establishing a requirement for *SIR2* in proper actin function. Moreover, deleting *SIR2* in a *bni1Δ* mutant further abrogated polarity defects as seen by extensive patch formation and actin aggregation in parallel to increased morphological aberrations, including cells displaying multiple buds (Figure 2D). In addition, we found that many *SIR2*-interacting genes have previously been shown to genetically interact with the essential genes *ACT1,* encoding actin, *MYO2*, encoding a type V myosin motor protein, and *RHO3*, a Rho-type GTPase involved in establishing cell polarity and Bni1p-dependent actin nucleation. The products of *ACT1, MYO2*, and *RHO3* interact physically with each other and also physically interact with many of the products of the genes shown here to interact with *SIR2* (Figure 2E), suggesting that *SIR2* itself might interact genetically with *ACT1*, *MYO2*, and *RHO3* (Boone et al., 2007; Kelley and Ideker, 2005; Tong et al., 2004). Indeed, *sir2Δ* cells display a markedly reduced fitness when combined with conditional actin mutation *act1-133* (Wertman et al., 1992) that reduces its ability to interact with myosin (Figures 2F and 2G) (Rayment et al., 1993; Smith et al., 1995). Moreover, conditional mutations (*myo2-14* and *myo2-16*) (Schott et al., 1999) in *MYO2* itself caused a drastically reduced fitness of *sir2Δ* cells (Figures 2F and 2G). No SS interaction was observed between *SIR2* and the other myosin genes, including *MYO3, MYO4*, and *MYO5* (not shown). *RHO3,* whose product, together with Bud6p, acts as an activator of Bni1p (Dong et al., 2003), was also found to interact genetically with *SIR2* (Figures 2E–2G).

To approach the question of whether the catalytic, deacetylating, activity of Sir2p is required for polarity functions, we tested if a wild-type Sir2p (pRS315-*SIR2*) and catalytically inactive Sir2p (pRS315-*SIR2(H364Y)*) (Moazed, 2001) could restore fitness of a *sir2Δ bni1Δ* double mutant subjected to Latranculin-B exposure. We found that only the catalytically proficient Sir2p was able to suppress Latranculin-B sensitivity (Figure 2H), demonstrating that deacetylase activity is required for Sir2p-dependent polarity functions.

It has been shown that Sir2p-independent life-span extension can be mediated by the Sir2p homolog Hst2p (Lamming et al., 2005) and that this latter sirtuin can, at least when overexpressed, compensate for the loss of Sir2p in genomic silencing (Perrod et al., 2001). Therefore, by performing SGA analysis with *HST2* as a query strain, we analyzed whether *HST2* displayed a global genetic interaction network similar to that of *SIR2*. To our surprise, we found that the genetic interaction network of *HST2* is vastly different from that of *SIR2.* In fact, only three genes, *YME1, TIM18,* and *CTF4,* are common to both networks and *HST2* did not show any synthetic genetic interaction with the genes required for proper actin cytoskeleton function or the polarisome (Table S4).

Sir2p Is Required for Efficient Folding of Actin by the Chaperonin CCT

As shown above, *SIR2* shares many genetic interactions with *ACT1*, indicating that actin function itself may be compromised in cells lacking Sir2p. Also, we found that *SIR2* interacted genetically with *cct6-18* (Figure 3A), an allele encoding a temperature-sensitive subunit of CCT (TriC). CCT, a member of the chaperonin subfamily of chaperones, is an essential oligomer formed from two back-to-back rings of eight subunits and is required for actin folding in vivo (reviewed by Brackley and Grantham, 2009). The folding activity of CCT in vivo has previously been assessed by utilizing the ability of native, monomeric actin to bind to DNaseI (Grantham et al., 2006; McLaughlin et al., 2002). Here we determined the conformational state of actin in wild-type and *sir2Δ* cells and found that cells lacking Sir2p displayed a reduced level of native actin while harboring the same total levels of actin as wild-type cells (Figures 3B and 3C). Both the concentration (Figure 3D) and the molar ratio of CCT subunit components (Figure 3E) were normal in cells lacking Sir2p. However, purified CCT from *sir2*Δ cells displayed elevated levels of acetylation (Figures 3F and 3G) and was much less efficient in folding actin than the wild-type CCT (Figures 3H and 3I).

The Polarisome and Myosin Motor Machinery Is Required for Mitotic Segregation of Protein Aggregates

Given that *SIR2* buffers against deficiencies in the machinery required for establishing proper polarity, we wondered if this machinery, like *SIR2*, partakes in the segregation of protein

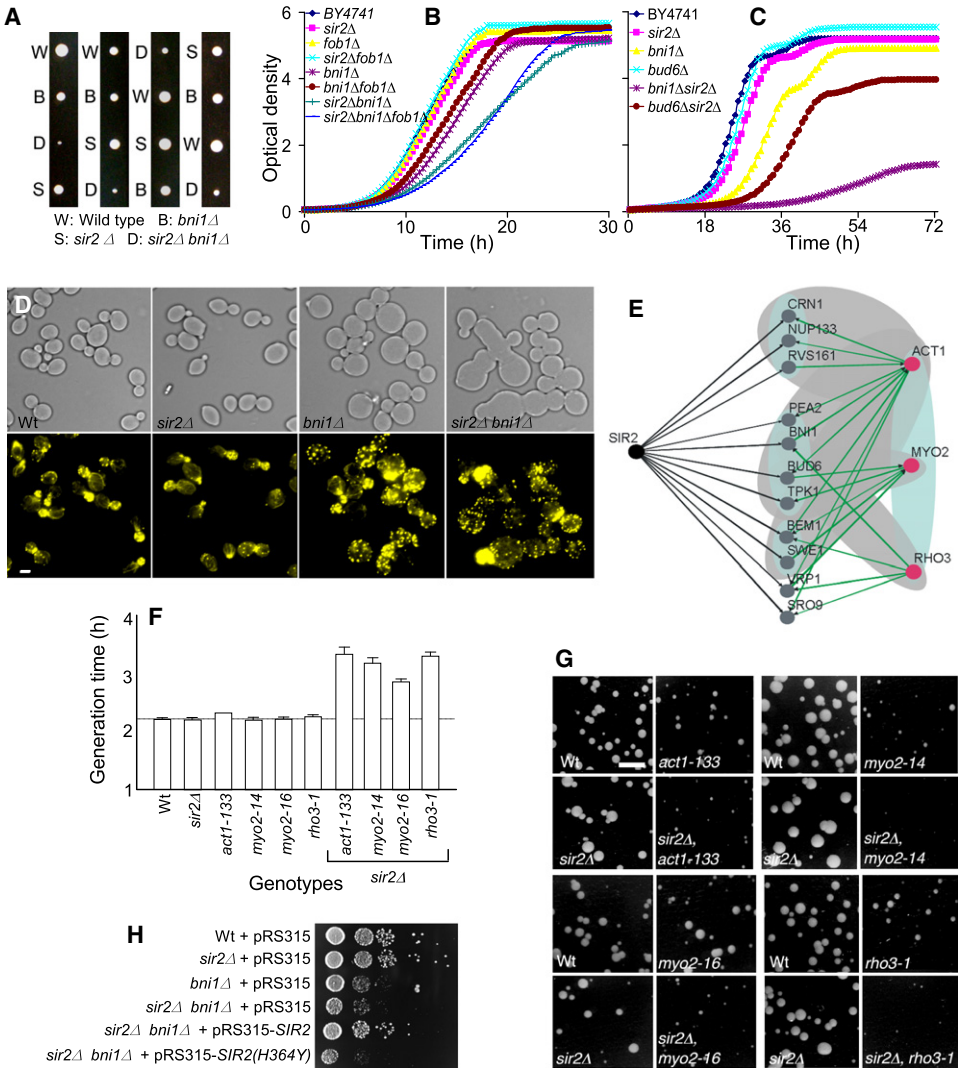

Figure 2. *SIR2* Interacts Genetically with Components of the Polarity and Myosin Motor Machinery

(A) Tetrad analysis confirmed the SS phenotype of the *sir2*Δ *bni1*Δ double mutant.

(B) A *sir2*Δ*bni1*Δ mutant reconstructed by PCR knockout displayed SS phenotype in liquid cultures (dark green line). The reduced growth of the *sir2Δ bni1Δ* was not linked to the accumulation of ERCs as the *fob1*Δ *sir2Δ bni1Δ* triple mutant (light blue line) showed similar phenotype as the double mutant.

(C) *bud6*Δ (brown line) or *bni1Δ* (purple line) harboring a *sir2Δ* deletion showed an increased sensitivity to the actin-depolarizing drug Latranculin-B.

(D) The *sir2Δ bni1Δ* double mutant shows extensive patch formation and actin aggregation in parallel to increased morphological aberrations. The strains, as indicated, were stained with rhodamine phalloidin (lower panel), and the upper panel shows bright-field images. Scale bars = 2 μm.

(E) Genetic interaction overlap and physical interaction data predict possible interactions between *SIR2* and *ACT1*, *MYO2*, and *RHO3*. Black edges are *SIR2* SS interactions found in this study and green edges are known genetic interactions with *ACT1, MYO2*, and *RHO3*. Published physical interactions are shown by shaded areas. Gray and light blue areas denote physical interactions within and between *SIR2* hits, respectively.

(F and G) SS interactions between *SIR2* and *ACT1* (*act1-133*), *MYO2* (*myo2-14* and *myo2-16*), and *RHO3* (*rho3-1*) temperature-sensitive mutations. (F) The generation times were compared at 30°C (*myo2-14*, *myo2-16*, and *rho3-1*) and 34°C (*act1-133*). Data are represented as mean ± standard deviation SD. (G) Random spore analysis of mutants as indicated was performed at 30°C. Scale bar = 4 mm (see also Table S4 for the full list of genetic interactions identified in the *HST2* SGA screen and the ones overlapping with *SIR2* interactions).

(H) Exponential phase cells were diluted to OD_{600} = 0.1 and plated on YPD medium with 10 μM Latranculin-B. The wild-type Sir2p (pRS315-*SIR2*) was able to suppress the Latranculin-B sensitivity of *sir2*Δ *bni1*Δ double mutants but not the catalytically inactive Sir2p (pRS315-*SIR2(H364Y)*).

damage during mitotic cytokinesis. To test this, we used an *a*ggregation *r*etention *e*fficiency (ARE, percentage of mother cells capable of retaining all aggregates during cytokinesis) assay. Cells were transiently heat shocked (42°C, 30 min) to trigger protein aggregation (Figures 4A and 4B), then returned to 30°C (no further aggregates formed) and the distribution of Hsp104-GFP-containing aggregates in mother and daughter compartments recorded during the next mitotic division event (Figures 4A and 4B). We first confirmed that heat-induced aggregates were retained in wild-type mother cells (Figures 4B and 4E)

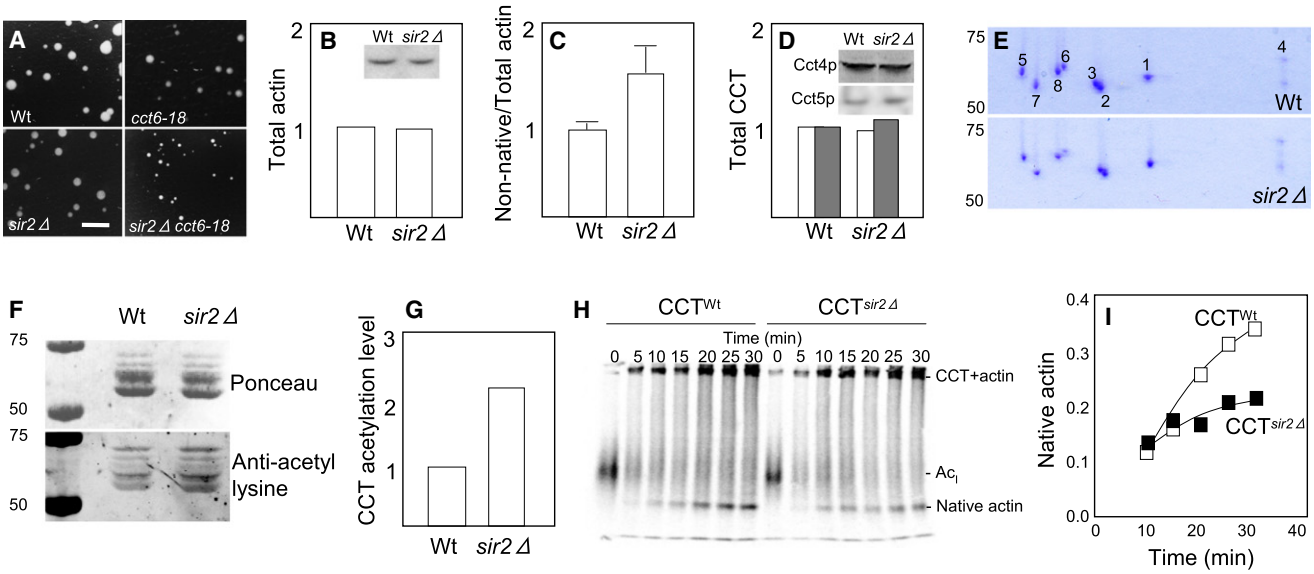

Figure 3. Cells Lacking Sir2p Contain Less Native Actin and Display Reduced CCT Activity

(A) Random spore analysis shows genetic SS interaction between SIR2 and CCT (cct6-18) at 30°C. Scale bar = 4 mm.

(B) Western blot analysis of whole lysates detected no differences in the total levels of actin between wild-type and *sir2Δ* cells.

(C) Depletion of native, monomeric actin from lysates via DNaseI-conjugated bead pull-down assays revealed an increase in the fraction of non-DNaseI-binding actin in the *sir2Δ* cells. Data are represented as mean ± SD.

(D) Western blot analysis of whole lysate confirmed that levels of CCT (Cct4p, probed by rabbit anti-TAP tag antibody from Upstate, white bars and Cct5p, probed by rat εAD2 antibody, gray bars) were equivalent between wild-type and *sir2Δ* cells, and purified CCT resolved by IEF-PAGE (pH gradient of 5 to 7 first dimension) revealed no differences in subunit composition (E).

(F) CCT in *sir2Δ* cells displays increased acetylation. Upper panel: Ponceau staining to confirm equal protein loading (19 μg/lane), and lower panel: signal from anti-acetyl lysine antibody.

(G) Quantification of signal from anti-acetyl lysine antibody (ImmuneChem ICP0380) using LI-CORE biosciences software with background subtraction.

(H and I) CCT purified from *sir2Δ* cells displays reduced folding activity. Human β-actin produced in an *E. coli* lysate in the presence of ^{35}S-methionine was used as a folding substrate for CCT purified from wild-type and *sir2Δ* cells. Time point samples were taken as indicated and resolved by native PAGE and phosphor-imaging. Counts representing actin bound to CCT, the input non-native actin folding intermediate (A_{cl}), and native actin are indicated and levels of native actin produced are shown in (I).

and that this segregation was less efficient in cells lacking *SIR2* (and *sir2Δ hmlΔ* mutants) but not those lacking *SIR3* or *SIR4* (Figures 4C and 4E). In addition, reduced ARE was not caused by ERC accumulation in the *sir2Δ* mutant as a *fob1*Δ mutation failed to suppress this defect (Figure 4E). It appears as if sustained Sir2p activity is important throughout the segregation process as adding the Sir2p inhibitor nicotinamide (NAM) both before and after heat shock reduced ARE (Figure 4F), although NAM added after a heat shock had a somewhat milder effect. Addition of NAM did not further reduce ARE in cells lacking Sir2p (Figure 4F). While abolishing or reducing Sir2p activity affected ARE negatively, adding resveratrol, a Sir2p activator (Howitz et al., 2003), boosted ARE by approximately 29% (Figure S2). However, introducing an extra copy of the *SIR2* gene did not result in increased ARE (not shown), suggesting that Sir2p activity is not, or is moderately, limiting for ARE in wild-type cells.

We then found that segregation of protein aggregates was less efficient in cells lacking different components of the polarity machinery shown to genetically interact with *SIR2*, including *BUD6* (Figure 4D), *BNI1*, *BEM1*, and *RVS161*, whereas the lack of the *BNR1* formin (no interaction with *SIR2*) had no effect on damage segregation (Figure 4E). The defect in aggregate segregation displayed by polarisome mutants was further abrogated (additively) by a *sir2*Δ deletion (Figure 4E). To confirm that heat-induced aggregates are segregated by the same mechanism as aging-induced aggregates, we isolated middle-aged mother cells (on average 7 generations old) and determined the ARE of wild-type and *bni1*Δ cells. As shown in Figure 4G, aggregates formed during aging instead of heat shock were also segregated in a Bni1p-dependent fashion.

The *act1-133* allele, which interacted genetically with *SIR2* (Figures 2F and 2G), caused a reduced binding of actin cables to myosin (Smith et al., 1995) and this mutation reduced the mother cells' ability to retain protein aggregates (Figure 4E), suggesting a role for the myosin V motor protein in damage segregation. Indeed, conditional *myo* alleles (*myo2-14* and *myo2-16*) (Schott et al., 1999) caused an almost complete breakdown of damage asymmetry (Figure 4E). Mother cells lacking Rho3p also failed to retain aggregates, further substantiating the involvement of the polarisome and the Myo2p motor protein in establishing cellular age asymmetry. None of the control strains (WT, *his3*Δ and WT, *ura6-4*) failed to partition protein aggregates under the same conditions (Figure 4E).

The breakdown of damage asymmetry was accompanied by a shorter *r*eplicative *l*ife *s*pan (RLS) of all polarity mutants

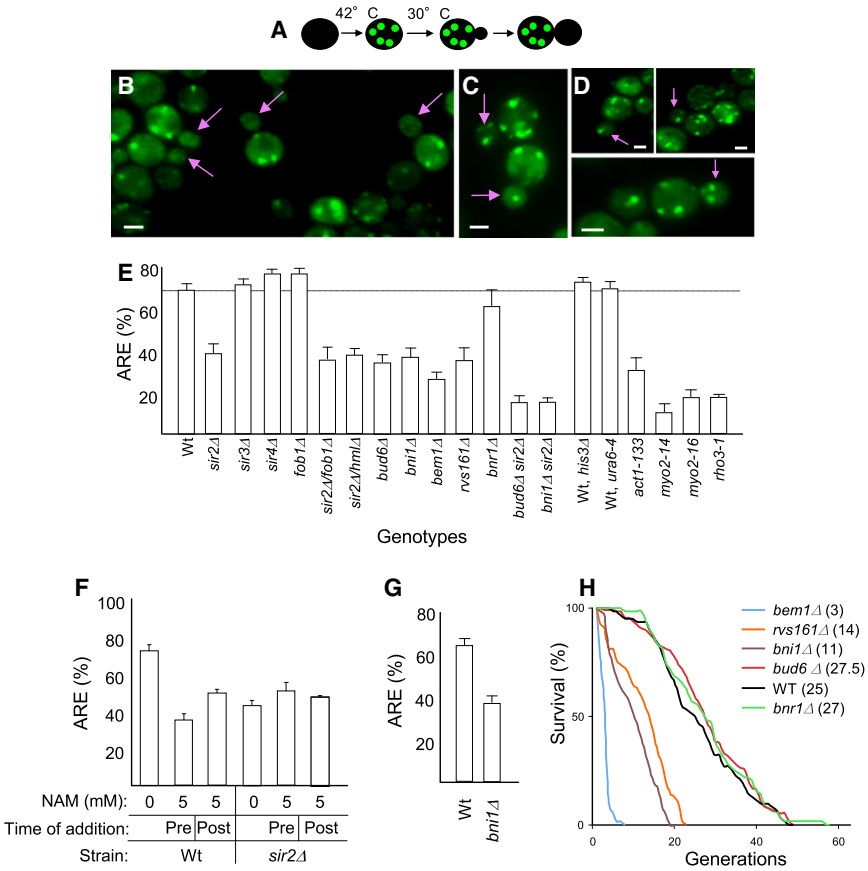

Figure 4. The Polarity and Myosin Motor Machinery Is Required for Mitotic Segregation of Protein Aggregates

(A) Schematic representation of the experimental design for determining the *a*ggregate *r*etention *e*fficiency (ARE).

(B, C, and D) Pictures showing aggregate partitioning during mitotic cytokinesis in wild-type (B), sir2Δ (C), and *bud6*Δ (D). Scale bars = 2 μm.

(E) ARE of mutants as indicated. (Data are represented as mean ± SD.)

(F) Wild-type and *sir2Δ* cells were treated with 5 mM of the Sir2p inhibitor nicotinamide (NAM) immediately prior to the heat shock (Pre) or directly after the heat shock (Post). Inhibiting Sir2p activity by adding NAM reduced ARE in WT but not in *sir2Δ* cells. (Data are represented as mean ± SD; see also Figure S2 for the Sir2p activator resveratrol test.)

(G) Middle-aged mother cells (on average 7 generation old) were isolated by magnetic sorting and the ARE were determined for wild-type and *bni1*Δ cells, demonstrating that aggregates formed during aging were also segregated in a Bni1p-dependent fashion. (Data are represented as mean ± SD.)

(H) Polarity mutants displayed a shorter RLS in comparison to the wild-type strain except for *bud6*Δ. Mean RLS is shown in parenthesis.

(*bni1Δ*, *bem1Δ*, and *rsv161Δ*) tested, except *bud6Δ* (Figure 4H). Lack of the septin-associated formin, Bnr1p, did not affect RLS (Figure 4H).

Daughter Cells Can Clear Themselves of Protein Aggregates by a Polarisome-Dependent Retrograde Transport

We next asked whether daughter cells can clear themselves of protein aggregates if such aggregates form by external stressors during cytokinesis. To test this, we developed an Hsp104-GFP aggregation clearance assay, in which we subjected cells to a 38°C heat shock and followed the localization of Hsp104p-containing aggregates. At this temperature, aggregates are constantly formed and resolved such that a steady-state level of aggregates is eventually reached. Immediately upon the heat shock, all cells displayed protein aggregates, including buds in the process of being formed by mother cells (Figure 5A). However, with time, aggregates disappeared from the buds but reappeared after daughter cells were released from the mother cell (single cells in Figure 5A). This clear out of aggregates required the polarisome formin Bni1p but not the septin-associated formin Bnr1p (Figure 5B). The data indicate that daughter cells can eliminate aggregates if the septum between mother and daughter is not closed and that this may be achieved by a retrograde flow of aggregates. Indeed, real-time imaging revealed that aggregates formed in the daughter compartment during heat shock relocalized into the mother cell (Figure 5C and Movies S1, S2, and S3). It is possible that actin patches and endocytosis play a role in this process as patches control Arp2/3-dependent movement of vesicles from the bud tip into the cell, which is retrograde from polarized secretion (Girao et al., 2008). However, we found that neither Arp2p nor Arp3p was required for aggregate clearance from buds whereas a mutation in the major tropomyosin gene *TPM1* severely reduced the efficiency of retrograde clearance (Figure 5D). Thus, retrograde flow of protein aggregates from the daughter cell to the mother cell appears to be an actin cable-dependent rather than actin patch-dependent process. In addition, Hsp104p-containing aggregates were localized to actin cable-rich rather than actin patch-rich regions (Figure 5E). We used a *p*roximity *l*igation *a*ssay (PLA) for detecting whether Hsp104p interacts with actin where a pair of oligonucleotide-labeled secondary antibodies (PLA probes) generates an individual fluorescent signal when bound to two primary antibodies in close proximity (Soderberg et al., 2006). We found that Hsp104p and actin interact in situ (Figure 5F and Figure S3), which further substantiates that segregation and retrograde flow of Hsp104p-associated aggregates depends on actin binding. As with segregation, retrograde flow of aggregates requires the Sir2p sirtuin but not Hst2p or Hst1p (Figure 5D).

Interestingly, the retrograde clearance of protein aggregates often ended with the daughter cell aggregate merging with a "receiving" aggregate in the mother cell (Figure 5C and Movies S1, S2, and S3). Whereas the Bnr1p formin was dispensable

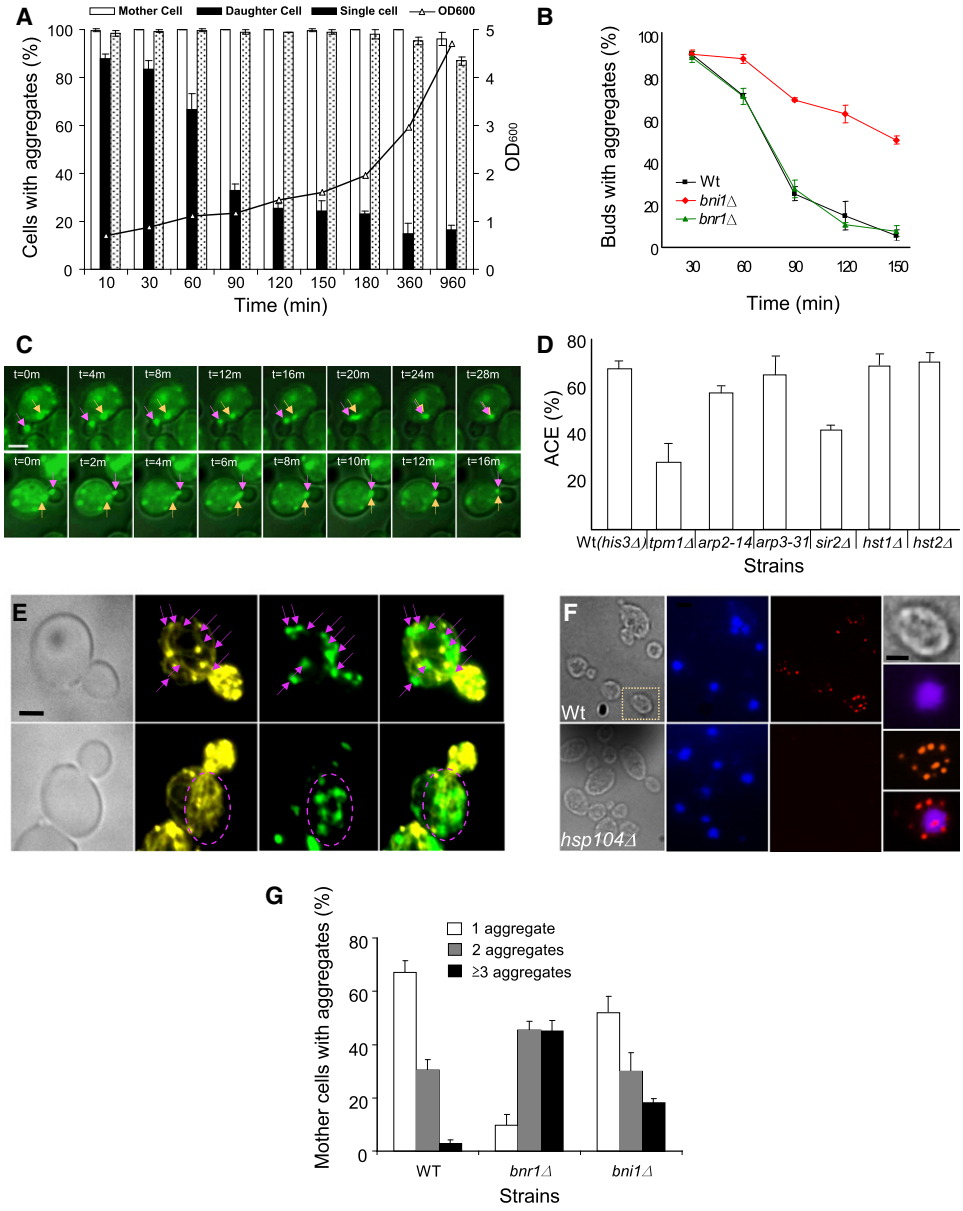

Figure 5. Daughter Cells Clear Themselves of Protein Aggregates by a Retrograde Transport during the Process of Cytokinesis

(A) Wild-type cells harboring an Hsp104-GFP chromosomal fusion were subjected to a 38°C heat treatment for 16 hr, and the localization of Hsp104-GFP-containing aggregates were followed in mother cells (white bars), their buds (still attached to mothers, black bars), and free single cells (detached from mothers, gray bars). The aggregates disappeared from the buds with time but were formed again after the daughter cells were released from the mother cell (single cells). Data are represented as mean ± SD.

(B) The formin Bni1p of the polarisome, but not the septin-associated formin Bnr1p, was required for the clearance of aggregates from daughters. Data are represented as mean ± SD.

(C) Real-time images of aggregates in heat-shocked cells. The pink arrows follow the movement of the aggregate formed in daughter cells until it reaches a receiving aggregate (yellow arrow) in the mother cell. Scale bars = 2 μm (see also Movies S1, S2, and S3).

(D) A mutant of the major tropomyosin gene TPM1 reduced the efficiency of retrograde clearance, but mutations in *ARP2* or *ARP3* did not, and retrograde flow of aggregates requires the Sir2p sirtuin but not Hst2p or Hst1p. Aggregate clearance efficiency (ACE) was calculated as % buds able to clear themselves of all aggregates in 90–150 min after heat shock (38°C). Data are represented as mean ± SD.

(E) Hsp104p-containing aggregates were localized to actin cable-rich regions (purple arrows and circle) rather than actin patch-rich regions. Images from left to right are bright-field, rhodamine phalloidin, Hsp104p-GFP, and rhodamine phalloidin-Hsp104p-GFP merged images of WT cells. Scale bars = 2 μm.

(F) Protein interactions between Hsp104p and actin in WT and *hsp104*Δ detected by the *p*roximity *l*igation *a*ssay (PLA). Images from left to right are bright field, Dapi, Cy3 (PLA signals). Scale bars = 2 μm (see also Figure S3 for the quantification data).

(G) Aggregate phenotype of BNI1 and BNR1 mutants after 90 min heat treatment (38°C). The absence of Bnr1p drastically reduced the merging of aggregates in mother cells. Data are represented as mean ± SD.

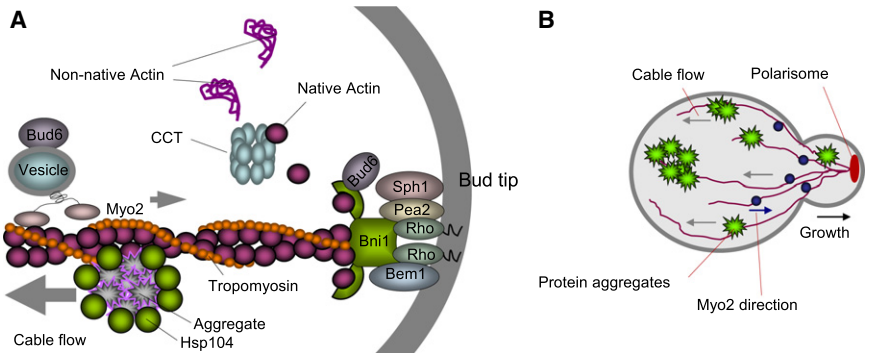

Figure 6. Model for Segregation and Retrograde Transport of Protein Aggregates

Schematic representation of the *SIR2*-interacting polarity machinery required for retention of protein aggregates (A) and a hypothetical model of the involvement of the polarisome in the retrograde transport and the retention of protein aggregates (B).

for the retrograde flow of aggregates (Figure 5B), its absence drastically reduced the merging of aggregates in mother cells (Figure 5G). Wild-type mother cells typically ended up with one large Hsp104-containing aggregate after 90 min at 38°C, whereas cells lacking Bnr1p displayed more than three aggregates (Figure 5G).

DISCUSSION

The differential inheritance of deleterious protein damage in sibling cells of microbes has been argued to imply that mandatory aging may have evolved in simple unicellular organisms (Ackermann et al., 2007; Nyström, 2007), and it was recently hypothesized that cellular polarization did not primarily evolve to drive morphogenesis but to restrict senescence to one daughter lineage in such organisms (Erjavec et al., 2008; Macara and Mili, 2008). If so, one would expect that some members of the polarity machinery have maintained their function in establishing unequal inheritance of protein damage, and this study provides support for this notion. Figure 6A schematically depicts the polarity machinery and gene products, of which all interacted with *SIR2*, found to be required for segregation of aggregates. Interestingly, Myo2p (required for proper inheritance of organelles) is also required for keeping the progeny free of protein aggregates. Since the direction of Myo2p movement is opposite to protein aggregates, this requirement of Myo2p may be due to Myo2p being needed for the transport of vesicles on which Bud6p, and possibly other proteins, hitchhike to the polarisome region (Jin and Amberg, 2000). Bud6p is required also for the segregation of ERCs, but this partitioning involves the septin ring (Shcheprova et al., 2008) rather than actin cables formed by the polarisome.

The involvement of the polarisome in the retention of protein aggregates could be a consequence of (1) actin cables providing a scaffold for large Hsp104p-containing aggregates (Erjavec et al., 2007; Ganusova et al., 2006), and (2) Bni1p-dependent nucleation of actin at the polarisome site resulting in a cable flow away from the bud tip ensuring that aggregates tethered on cables will not enter the bud (Figure 6B). In addition, we found that aggregates formed upon heat stress in emerging buds were transported back to the mother cell, establishing a new polarity mechanism that goes opposite to the flow associated with actin-based polarized secretion, which is directed by motor movement along actin cables. This, we believe, is the first documentation of polarized flow of material from the daughter to the mother (Figure 5C and Movies S1, S2, and S3). The data showing that the transport of aggregates into mother cells is tropomyosin dependent but not Arp2/3 dependent demonstrate that this retrograde flow is actin cable dependent. However, it is not clear if transport of aggregates is entirely due to actin cable association and actin retrograde flow since the rate of extension of the tip of an elongating actin cable is 0.29 ± 0.08 μm per second (Yang and Pon, 2002) and aggregate movement into mother cells appears to be slower. However the rate of movement of aggregates into mother cells also depends on the rate at which the actin nucleation center at the bud tip moves away from the mother-daughter septum area. In addition, it is not known how the association of large aggregates affects actin cable dynamics and retrograde flow nor do we know if cable function and retrograde flow are affected by the heat shock treatment applied. Thus, the rate measurements neither exclude nor support that the transport of aggregates is entirely due to actin retrograde flow.

Aggregates translocated from the daughter cell compartment were found to merge with aggregates in the mother cell, and with time the heat-stressed cells ended up with an average of one large Hsp104p-containing aggregate. Interestingly, this merging of aggregates required the formin, Bnr1p, of the septin ring rather than Bni1p (Figure 5G). Thus, the two formins of yeast have distinct roles in the spatial management of protein aggregates; one, Bni1p, provides the organism with the means to retain (in mother cells) and translocate (into mother cells) aggregates, whereas the other, Bnr1p, allows aggregates to merge into a single large inclusion body. This latter process is somewhat similar to aggresome formation but is distinct in that aggresomes are formed via the microtubule network and dynein motors and are associated with the centrosome (spindle pole body in yeast) (Johnston et al., 1998; Wang et al., 2009), whereas the Hsp104p-associated aggregates formed upon aging and stress are associated with the actin cytoskeleton and are dependent on actin nucleation. Nevertheless, both processes appear to be regulated, in part, by deacetylases, aggresome formation by HDAC6 (Kawaguchi et al., 2003), and the translocation of Hsp104p-recognized aggregates by Sir2p.

The role of Sir2p in establishing proper polarity and cytoskeletal functions appears linked to the sirtuin being required for CCT function. It has been shown previously that a point mutation in the Cct4p subunit results in an abnormal actin cytoskeleton at

the nonpermissive temperature (Vinh and Drubin, 1994). This mutation ($G_{345}D$) resides on the outside face of the apical substrate-binding domain (Llorca et al., 1999) and has been shown to affect the allostery of the CCT ATPase and reduce its ability to fold actin (Shimon et al., 2008). In similar assays we observed that CCT purified from *sir2Δ* cells is much less efficient at folding actin than CCT purified from wild-type cells and carried a heavier load of acetylated lysines. It would therefore appear from both this study and the work of Shimon et al. (2008) that relatively small changes to the CCT oligomer (such as posttranslational modifications and point mutations) have the potential to disrupt its activity. In line with this, the DNaseI pull-down assays revealed an increase in the levels of non-native actin in the *sir2Δ* cells. A similar result was observed in mammalian cells when CCT levels were reduced by siRNA (Grantham et al., 2006). However, it is unclear if the elevated levels of CCT acetylation in *sir2Δ* cells are the cause of its reduced activity or whether CCT is a direct target for Sir2p-dependent deacetylation. Nevertheless, its reduced folding activity in *sir2Δ* cells explains the extensive overlap between the genetic interaction network of *SIR2* and *ACT1* and why *sir2Δ* mutants display subtle polarity defects.

Hsp104p could also affect polarity in *sir2Δ* cells as Hsp104p-dependent functions are reduced in cells lacking the sirtuin (Erjavec et al., 2007) and Spa2p, a member of the polarisome, is a substrate for Hsp104p, identified using a dominant-negative variant of Hsp104p, HAP/ClpP, that degrades substrates instead of remodeling them (Tessarz et al., 2009). HAP/ClpP expression affects the integrity of the actin cytoskeleton and Spa2-dependent localization of Pea2p to the bud tip fails (Tessarz et al., 2009). However, as Pea2p is properly localized in cells totally lacking Hsp104p (Tessarz et al., 2009), the reduced activity of Hsp104p in *sir2Δ* cells is unlikely to contribute substantially to polarity defects in this mutant. The *SPA2* gene was not identified in our original *SIR2* SGA screen, but random spore analysis confirmed that *SIR2* and *SPA2* show a genetic SS interaction (not shown).

Segregation of damaged/aggregated proteins and accumulation of ERCs are both processes subjected to control by Sir2p and, in addition to dysfunctional mitochondria (Lai et al., 2002; Veatch et al., 2009), it is possible that proteotoxic aggregates and ERCs are aging factors in mitotic yeast that contribute to replicative aging. In addition, Sir2p is required for the maintenance of telomeric chromatin in aging cells (Dang et al., 2009). These multiple roles of Sir2p could explain why *sir2* deletions have a negative effect on yeast replicative life span in cells lacking Fob1p (Kaeberlein et al., 1999), in which formation of ERCs is drastically reduced, and suggest that Sir2p controls life span also in an ERC-independent manner. One such ERC-independent function important for longevity may be the control of cytoskeletal functions and polarity. All polarity mutants tested, except *bud6Δ* cells, displayed accelerated aging, but it is presently unclear to what extent this may be due to failures in damage segregation or to general polarity defects. However, the reduced life span does not correlate to general fitness defects (reduced growth rate) given that, for example, the *rvs161Δ* mutant displayed no fitness defect but a drastically accelerated aging whereas *bnr1Δ* and *bud6Δ* mutants show decreased fitness but a normal life span. It is possible that the residual activity of Bni1p in *bud6Δ* cells is enough to maintain proper polarity and longevity, but this seems unlikely as *bud6Δ* and *bni1Δ* mutants displayed a similar defect in the segregation of protein aggregates. An alternative, and entirely speculative, possibility is that the effects observed for ERC segregation in cells deficient for Bud6p (Shcheprova et al., 2008) counteract, or mask, failure to partition aggregates.

The data presented raises the questions of whether spatial protein quality control operates during mitosis (or meiosis) in specific cells and tissues of higher organisms, if there are dedicated waste-disposal cells in these organisms, and if the efficiency of SQC affects the onset of age-related proteotoxic maladies, such as familial and sporadic neurodegeneration.

EXPERIMENTAL PROCEDURES

Strains and Plasmids

Strains, primers, and plasmids are described in the Extended Experimental Procedures and Tables S1 and S2.

SIR2 Query Strain Construction and Synthetic Genetic Array Analysis

To apply the SGA method to the *SIR2* screen, the *HMR* and *HML* loci in a *sir2Δ* *MATα* haploid background were deleted by PCR knockout. Query strain construction, interaction confirmation, and functional enrichment analysis are described in the Extended Experimental Procedures.

Latranculin-B Sensitivity Test

Latrunculin-B (2 mM in DMSO stock solution) was added to the medium to a final concentration of 15 μM, a concentration at which the wild-type strain showed a growth rate decrease of about 20%. The same amount of DMSO was added to the control set.

Actin Staining

Actin staining with rhodamine phalloidin (Invitrogen) was preformed using standard protocols.

CCT Purification and Folding Assays

CCT oligomers were purified using a TAP-tag procedure described in the Extended Experimental Procedures. Folding assays were carried out essentially as described by Pappenberger et al. (2006). Counts corresponding to native actin in each lane were standardized to the Coomassie signal of the CCT band to account for any slight variations in gel loading.

DNaseI-Binding Assays

DNaseI-binding assays were performed in triplicate as described in the Extended Experimental Procedures.

Hsp104-GFP Aggregation Retention Efficiency assay

Cells expressing an Hsp104-GFP chromosomal fusion were grown to mid-log phase (optical density [OD] 600 ≈ 0.5) in YPD medium at 30°C (22°C for temperature-sensitive [TS] mutants) and then shifted to 42°C heat shock for 30 min. Cells were transferred back to 30°C for recovery and samples (2 ml aliquots) were taken in triplicate every 10 min for analysis of inheritance of aggregates by using a Zeiss fluorescence microscope.

Hsp104-GFP Aggregation Clearance Assay

Hsp104-GFP-containing mid-log phase cells were shifted to 38°C for 16 hr (aggregates will keep forming in the cell at this temperature). Aggregate clearance efficiency (ACE) was calculated as percentage of buds able to clear themselves of all aggregates in 90–150 min after heat shock.

Nicotinamide and Resveratrol Treatment

Nicotinamide (final concentration 5 mM) was added 10 min before heat shock treatment and directly after heat shock treatment. Resveratrol (final concentration 200 μM) was added to cultures 10 min before heat shock. The same amount of ethanol was added to the control.

Isolation of Old Cells

Old mother cells were obtained by magnetic sorting as described previously (Smeal et al., 1996).

Life-Span Analysis

Replicative life span was determined using a micromanipulator (Singer Instruments) and following standard protocols.

Time-Lapse Fluorescence Imaging

Cells were grown in YPD until mid-log phase (OD_{600} = 0.5) at 30°C. Aggregates were induced with heat shock at 42°C as explained previously, and then cells were recovered for 10 min at 30°C and 5 min at 23°C. Images were acquired every minute for 30–40 min. QuickTime movies were made from time-lapse images using GraphicsGale version 1.93.07.

Detection of Protein Interactions by In Situ Proximity Ligation Assay

Mid-log phase BY4741 and *hsp104*Δ strains were heat shocked (20 min) to induce Hsp104p expression. Primary antibodies were the rabbit anti-Hsp104 polyclonal antibody (MBL) and the mouse anti-actin (clone 4) monoclonal antibody (Seven Hills Bioreagents). Cells were harvested and pretreated based on standard immunofluoresence staining protocols with modifications, and the PLA assay performed as described previously by Soderberg et al. (2006). PLA signals were detected with a Duolink PLA detection kit 563.

SUPPLEMENTAL INFORMATION

Supplemental Information includes Extended Experimental Procedures, three figures, four tables, and three movies and can be found with this article online at doi:10.1016/j.cell.2009.12.031.

ACKNOWLEDGMENTS

The authors would like to thank Charles Boone for providing strains, software support for the SGA analysis, and helpful suggestions throughout this work. The εAD2 antibody was a kind gift from Keith Willison, and David Sinclair provided useful information on reagents and antibodies. This work was supported by grants from the Swedish Natural Research Council (VR), the Wallenberg scholar award, the Foundation for Strategic Research in Sweden (SSF-BioX program), the Göran Gustafsson Foundation, and the EC (Acronyms: Mimage & Proteomage).

Received: June 25, 2009
Revised: October 13, 2009
Accepted: December 16, 2009
Published: January 21, 2010

REFERENCES

Ackermann, M., Chao, L., Bergstrom, C.T., and Doebeli, M. (2007). On the evolutionary origin of aging. Aging Cell *6*, 235–244.

Ackermann, M., Stearns, S.C., and Jenal, U. (2003). Senescence in a bacterium with asymmetric division. Science *300*, 1920.

Aguilaniu, H., Gustafsson, L., Rigoulet, M., and Nystrom, T. (2003). Asymmetric inheritance of oxidatively damaged proteins during cytokinesis. Science *299*, 1751–1753.

Barker, M.G., and Walmsley, R.M. (1999). Replicative ageing in the fission yeast *Schizosaccharomyces pombe*. Yeast *15*, 1511–1518.

Boone, C., Bussey, H., and Andrews, B.J. (2007). Exploring genetic interactions and networks with yeast. Nat. Rev. Genet. *8*, 437–449.

Brackley, K.I., and Grantham, J. (2009). Activities of the chaperonin containing TCP-1 (CCT): implications for cell cycle progression and cytoskeletal organisation. Cell Stress Chaperones *14*, 23–31.

Dang, W., Steffen, K.K., Perry, R., Dorsey, J.A., Johnson, F.B., Shilatifard, A., Kaeberlein, M., Kennedy, B.K., and Berger, S.L. (2009). Histone H4 lysine 16 acetylation regulates cellular lifespan. Nature *459*, 802–807.

Defossez, P.-A., Prusty, R., Kaeberlein, M., Lin, S.-J., Ferrigno, P., Silver, P.A., Keil, R.L., and Guarente, L. (1999). Elimination of replication block protein Fob1 extends the life span of yeast mother cells. Mol. Cell *3*, 447–455.

Dong, Y., Pruyne, D., and Bretscher, A. (2003). Formin-dependent actin assembly is regulated by distinct modes of Rho signaling in yeast. J. Cell Biol. *161*, 1081–1092.

Erjavec, N., and Nyström, T. (2007). Sir2p-dependent protein segregation gives rise to a superior reactive oxygen species management in the progeny of *Saccharomyces cerevisiae*. Proc. Natl. Acad. Sci. USA *104*, 10877–10881.

Erjavec, N., Larsson, L., Grantham, J., and Nyström, T. (2007). Accelerated aging and failure to segregate damaged proteins in Sir2 mutants can be suppressed by overproducing the protein aggregation-remodeling factor Hsp104p. Genes Dev. *21*, 2410–2421.

Erjavec, N., Cvijovic, M., Klipp, E., and Nyström, T. (2008). Selective benefits of damage partitioning in unicellular systems and its effects on aging. Proc. Natl. Acad. Sci. USA *105*, 18764–18769.

Ganusova, E.E., Ozolins, L.N., Bhagat, S., Newnam, G.P., Wegrzyn, R.D., Sherman, M.Y., and Chernoff, Y.O. (2006). Modulation of prion formation, aggregation, and toxicity by the actin cytoskeleton in yeast. Mol. Cell. Biol. *26*, 617–629.

Girao, H., Geli, M.I., and Idrissi, F.Z. (2008). Actin in the endocytic pathway: from yeast to mammals. FEBS Lett. *582*, 2112–2119.

Grantham, J., Brackley, K.I., and Willison, K.R. (2006). Substantial CCT activity is required for cell cycle progression and cytoskeletal organization in mammalian cells. Exp. Cell Res. *312*, 2309–2324.

Guarente, L. (2000). Sir2 links chromatin silencing, metabolism, and aging. Genes Dev. *14*, 1021–1026.

Howitz, K.T., Bitterman, K.J., Cohen, H.Y., Lamming, D.W., Lavu, S., Wood, J.G., Zipkin, R.E., Chung, P., Kisielewski, A., Zhang, L.L., et al. (2003). Small molecule activators of sirtuins extend *Saccharomyces cerevisiae* lifespan. Nature *425*, 191–196.

Imai, S.-i., Armstrong, C.M., Kaeberlein, M., and Guarente, L. (2000). Transcriptional silencing and longevity protein Sir2 is an NAD-dependent histone deacetylase. Nature *403*, 795–800.

Jin, H., and Amberg, D.C. (2000). The secretory pathway mediates localization of the cell polarity regulator Aip3p/Bud6p. Mol. Biol. Cell *11*, 647–661.

Johnston, J.A., Ward, C.L., and Kopito, R.R. (1998). Aggresomes: A cellular response to misfolded proteins. J. Cell Biol. *143*, 1883–1898.

Kaeberlein, M., McVey, M., and Guarente, L. (1999). The *SIR2/3/4* complex and *SIR2* alone promote longevity in *Saccharomyces cerevisiae* by two different mechanisms. Genes Dev. *13*, 2570–2580.

Kaeberlein, M., Burtner, C.R., and Kennedy, B.K. (2007). Recent developments in yeast aging. PLoS Genet. *3*, e84.

Kawaguchi, Y., Kovacs, J.J., McLaurin, A., Vance, J.M., Ito, A., and Yao, T.P. (2003). The deacetylase HDAC6 regulates aggresome formation and cell viability in response to misfolded protein stress. Cell *115*, 727–738.

Kelley, R., and Ideker, T. (2005). Systematic interpretation of genetic interactions using protein networks. Nat. Biotechnol. *23*, 561–566.

Kirkwood, T.B.L. (1977). Evolution of ageing. Nature *270*, 301–304.

Kirkwood, T.B.L. (1981). Repair and Its Evolution: Survival versus Reproduction (Oxford: Blackwell Scientific Publications).

Kirkwood, T.B.L., and Holliday, R. (1979). The evolution of ageing and longevity. Proc. R. Soc. Lond. B Biol. Sci. *205*, 531–546.

Lai, C.Y., Jaruga, E., Borghouts, C., and Jazwinski, S.M. (2002). A mutation in the *ATP2* gene abrogates the age asymmetry between mother and daughter cells of the yeast *Saccharomyces cerevisiae*. Genetics *162*, 73–87.

Lamming, D.W., Latorre-Esteves, M., Medvedik, O., Wong, S.N., Tsang, F.A., Wang, C., Lin, S.J., and Sinclair, D.A. (2005). *HST2* mediates *SIR2*-independent life-span extension by calorie restriction. Science *309*, 1861–1864.

Lindner, A.B., Madden, R., Demarez, A., Stewart, E.J., and Taddei, F. (2008). Asymmetric segregation of protein aggregates is associated with cellular aging and rejuvenation. Proc. Natl. Acad. Sci. USA *105*, 3076–3081.

Llorca, O., McCormack, E.A., Hynes, G., Grantham, J., Cordell, J., Carrascosa, J.L., Willison, K.R., Fernandez, J.J., and Valpuesta, J.M. (1999). Eukaryotic type II chaperonin CCT interacts with actin through specific subunits. Nature *402*, 693–696.

Macara, I.G., and Mili, S. (2008). Polarity and differential inheritance universal attributes of life? Cell *135*, 801–812.

McLaughlin, S., Wang, J., Gambhir, A., and Murray, D. (2002). PIP2 and PROTEINS: Interactions, organization, and information flow. Annu. Rev. Biophys. Biomol. Struct. *31*, 151–175.

Moazed, D. (2001). Enzymatic activities of Sir2 and chromatin silencing. Curr. Opin. Cell Biol. *13*, 232–238.

Moseley, J.B., and Goode, B.L. (2006). The yeast actin cytoskeleton: from cellular function to biochemical mechanism. Microbiol. Mol. Biol. Rev. *70*, 605–645.

Nyström, T. (2007). A bacterial kind of aging. PLoS Genet. *3*, e224.

Pappenberger, G., McCormack, E.A., and Willison, K.R. (2006). Quantitative actin folding reactions using yeast CCT purified via an internal tag in the CCT3/gamma subunit. J. Mol. Biol. *360*, 484–496.

Partridge, L., and Barton, N.H. (1993). Optimality, mutation and the evolution of ageing. Nature *362*, 305–311.

Perrod, S., Cockell, M.M., Laroche, T., Renauld, H., Ducrest, A.L., Bonnard, C., and Gasser, S.M. (2001). A cytosolic NAD-dependent deacetylase, Hst2p, can modulate nucleolar and telomeric silencing in yeast. EMBO J. *20*, 197–209.

Pruyne, D., Evangelista, M., Yang, C., Bi, E., Zigmond, S., Bretscher, A., and Boone, C. (2002). Role of formins in actin assembly: Nucleation and barbed-end association. Science *297*, 612–615.

Rayment, I., Holden, H.M., Whittaker, M., Yohn, C.B., Lorenz, M., Holmes, K.C., and Milligan, R.A. (1993). Structure of the actin-myosin complex and its implications for muscle contraction. Science *261*, 58–65.

Rogina, B., and Helfand, S.L. (2004). Sir2 mediates longevity in the fly through a pathway related to calorie restriction. Proc. Natl. Acad. Sci. USA *101*, 15998–16003.

Sagot, I., Rodal, A.A., Moseley, J., Goode, B.L., and Pellman, D. (2002). An actin nucleation mechanism mediated by Bni1 and profilin. Nat. Cell Biol. *4*, 626–631.

Schott, D., Ho, J., Pruyne, D., and Bretscher, A. (1999). The COOH-terminal domain of Myo2p, a yeast myosin V, has a direct role in secretory vesicle targeting. J. Cell Biol. *147*, 791–808.

Shcheprova, Z., Baldi, S., Frei, S.B., Gonnet, G., and Barral, Y. (2008). A mechanism for asymmetric segregation of age during yeast budding. Nature *454*, 728–734.

Shimon, L., Hynes, G.M., McCormack, E.A., Willison, K.R., and Horovitz, A. (2008). ATP-induced allostery in the eukaryotic chaperonin CCT is abolished by the mutation G345D in CCT4 that renders yeast temperature-sensitive for growth. J. Mol. Biol. *377*, 469–477.

Sinclair, D.A. (2002). Paradigms and pitfalls of yeast longevity research. Mech. Ageing Dev. *123*, 857–867.

Sinclair, D.A., and Guarente, L. (1997). Extrachromosomal rDNA circles–A cause of aging in yeast. Cell *91*, 1033–1042.

Smeal, T., Claus, J., Kennedy, B., Cole, F., and Guarente, L. (1996). Loss of transcriptional silencing causes sterility in old mother cells of *S. cerevisiae*. Cell *84*, 633–642.

Smith, M.G., Simon, V.R., O'Sullivan, H., and Pon, L.A. (1995). Organelle-cytoskeletal interactions: actin mutations inhibit meiosis-dependent mitochondrial rearrangement in the budding yeast *Saccharomyces cerevisiae*. Mol. Biol. Cell *6*, 1381–1396.

Soderberg, O., Gullberg, M., Jarvius, M., Ridderstrale, K., Leuchowius, K.-J., Jarvius, J., Wester, K., Hydbring, P., Bahram, F., Larsson, L.-G., and Landegren, U. (2006). Direct observation of individual endogenous protein complexes in situ by proximity ligation. Nat. Methods *3*, 995–1000.

Stewart, E.J., Madden, R., Paul, G., and Taddei, F. (2005). Aging and death in an organism that reproduces by morphologically symmetric division. PLoS Biol. *3*, e45.

Tessarz, P., Schwarz, M., Mogk, A., and Bukau, B. (2009). The yeast AAA+ chaperone Hsp104 is part of a network that links the actin cytoskeleton with the inheritance of damaged proteins. Mol. Cell Biol. *29*, 3738–3745.

Tissenbaum, H.A., and Guarente, L. (2001). Increased dosage of a sir-2 gene extends lifespan in *Caenorhabditis elegans*. Nature *410*, 227–230.

Tong, A.H., Evangelista, M., Parsons, A.B., Xu, H., Bader, G.D., Page, N., Robinson, M., Raghibizadeh, S., Hogue, C.W., Bussey, H., et al. (2001). Systematic genetic analysis with ordered arrays of yeast deletion mutants. Science *294*, 2364–2368.

Tong, A.H., Lesage, G., Bader, G.D., Ding, H., Xu, H., Xin, X., Young, J., Berriz, G.F., Brost, R.L., Chang, M., et al. (2004). Global mapping of the yeast genetic interaction network. Science *303*, 808–813.

Veatch, J.R., McMurray, M.A., Nelson, Z.W., and Gottschling, D.E. (2009). Mitochondrial dysfunction leads to nuclear genome instability via an iron-sulfur cluster defect. Cell *137*, 1247–1258.

Vinh, D.B., and Drubin, D.G. (1994). A yeast TCP-1-like protein is required for actin function in vivo. Proc. Natl. Acad. Sci. USA *91*, 9116–9120.

Wang, Y., Meriin, A.B., Zaarur, N., Romanova, N.V., Chernoff, Y.O., Costello, C.E., and Sherman, M.Y. (2009). Abnormal proteins can form aggresome in yeast: aggresome-targeting signals and components of the machinery. FASEB J. *23*, 451–463.

Warringer, J., Ericson, E., Fernandez, L., Nerman, O., and Blomberg, A. (2003). High-resolution yeast phenomics resolves different physiological features in the saline response. Proc. Natl. Acad. Sci. USA *100*, 15724–15729.

Weismann, A. (1889). Essays upon Heredity and Kindred Biological Problems (Oxford: Clarendon Press).

Wertman, K.F., Drubin, D.G., and Botstein, D. (1992). Systematic mutational analysis of the yeast *ACT1* gene. Genetics *132*, 337–350.

Yang, H.C., and Pon, L.A. (2002). Actin cable dynamics in budding yeast. Proc. Natl. Acad. Sci. USA *99*, 751–756.

Cell

EXTENDED EXPERIMENTAL PROCEDURES

Strains and Plasmids

Yeast strains used in this study and primers for strain construction are listed in Tables S1 and S2. Briefly, the strain Y7092 was used as the SGA starting strain for query strain constructions and Y8835 was the "wild-type" control strain for the *natR*-marked query strain. The SGA-v2 *MAT***a** deletion strains collection, temperature-sensitive (TS) mutants (*act1-133*, *myo2-14*, *myo2-16*, and *rho3-1*) and the two strains mentioned above were obtained from Charles Boone. Plasmids p4339, YDpU, pAG32 and pRS315 were used to amplify the *natMX4*, *URA3*, *hphMX4* and *LEU2* cassettes, respectively. Plasmids pRS315-*SIR2* and pRS315-*SIR2(H364Y)* were used to test the dependence of Sir2p deacetylase activity for the SS interaction observed between *SIR2* and *BNI1*. The deletion mutants expressing Hsp104-GFP or CCT4-TAP from the chromosomal locus were constructed by standard PCR knock-out methodology. The TS Hsp104-GFP strains were constructed by crossing an Hsp104-GFP *LEU2* strain (Y7092 background) with the TS mutants (BY4741 background) followed by selection for TS and Hsp104-GFP LEU2 in the *MAT***a** progeny.

SIR2 Query Strain Construction and Synthetic Genetic Array Analysis

The methodology of SGA analysis involves a series pinning replicate procedures. Mating, meiotic recombination and the SGA reporter (*can1*Δ*::STE2pr-Sp_his5*) are used to convert the single mutant input array into a double mutant output array (Boone et al., 2007). The *sir2Δ* haploid strain is sterile due to loss of silencing at the silent mating type loci, *HML* and *HMR,* which result in coexpression of *MAT*α and *MAT***a** mating type information (Ivy et al., 1986; Rine and Herskowitz, 1987). In order to apply the SGA method for the an *SIR2* screen, the *HMR* locus in a *sir2*Δ *MAT*α haploid background was deleted by PCR knockout and to allow the selection for the *MAT***a** haploid by the SGA reporter the *HML* locus in the same background was also deleted. The query strain Ysir2-srl was confirmed by 8 pairs of primers, which were designed to confirm the deletion at the *SIR2*, *HMR* and *HML* loci and the integrity of the *MAT*α locus. The SGA screen was performed in duplicate as described (Tong et al., 2001; Tong et al., 2004). The screen was run in 1536-spot format by using a SINGER ROTOR HDA Robot (Singer Instrument Co. Ltd.). SGA hits with the highest statistical probability to be true interactions were confirmed by the Bioscreen assay (Warringer et al., 2003).

Confirmation of Genetic Interaction by Bioscreen Assay, Tetrad Dissection Analysis, and Random Spore Analysis

The microcultivation experiments were performed in triplicate by using the Bioscreen C equipment (Labsystems Oy, Helsinki, Finland) in which optical density was measured every 20 min for 47 hr. The LSC (Logarithmic Strain Coefficient) values of growth rate, lag phase and yield were calculated as described (Warringer et al., 2003), and its statistical significance tested using a two tails student's t test and a threshold test. The significant ones fulfilled both tests (t test ($p \leq 0, 05$) and the threshold test: LSC difference higher than 3 times the standard error). Genetic interaction between *BNI1* and *SIR2* was verified by tetrad dissection. The genetic make-up of the double mutants was inferred by replica plating the colonies on selective medium (containing nourseothricin, for *sir2*Δ*::natMX4* cells, and kanamycin, for the *bni1*Δ*::kanMX4* mutant selection). Random spore analysis was preformed as described (Tong et al., 2001; Tong et al., 2004) at 26, 28, 30, 32 and 34°C to check the double mutant phenotypes of *SIR2* and TS mutants.

Functional Enrichment and Interaction Network Analysis

The functional enrichment analysis was based on the result from Gene Ontology Term Finder (Boyle et al., 2004), and p values were calculated by using a hypergeometric distribution with Multiple Hypothesis Correction. Bioscreen-confirmed hits were analyzed for the enrichment of GO-bioprocesses groups by comparing to a background set list of SGA-V2 array (4261 genes) with a p value cut-off $p < 0. 01$. The *SIR2* network diagrams were extracted from the interaction analysis by using Ospery 1.2.0 (Breitkreutz et al., 2003) and the physical interactions between SGA hits were added according to the BioGRID interaction database (Breitkreutz et al., 2008).

Latranculin-B Sensitivity Test

Latrunculin-B (2 mM in DMSO stock solution) was added to the medium to a final concentration of 15 μM, a concentration where the wild-type strain showed a growth rate decrease of about 20%. The same amount of DMSO was added to the control set. Growth was checked by the Bioscreen microcultivation approach with five different replicas. The optical density (OD) was measured every 30 min for 72 hr.

Actin Staining

Actin staining with rhodamine phalloidin (Invitrogen) was preformed using standard protocols. Images were acquired with bright-field, rhodamine, and GFP channels by using a Zeiss Axiovert 200 M fluorescence microscope.

CCT Purification and Folding Assays

CCT oligomer was purified via a TAP-tag situated at the extreme C terminus of Cct4p first by Protein A affinity binding to IgG Sepharose beads followed by cleavage of the tag at the TEV protease site. Subsequent purification was achieved via the calmodulin-binding peptide using standard protocols.

Purified CCT was dialyzed against CCT buffer (10 mM HEPES [pH 8.0], 150 mM KCl, 1 mM DTT, 50% glycerol) and concentrated using an Amicon Ultra-4 concentrating unit. Folding assays were carried out essentially as described by (Pappenberger et al., 2006)

using human β-actin expressed in an *E. coli* lysate (Novagen EcoPro T7), in the presence of ^{35}S-methionine. The folding reactions contained 220 μg CCT and were carried out at 30°C. Time point samples were taken and stored on ice until being resolved on a pre-cooled 6% Native gel (Liou and Willison, 1997) containing 1 mM ATP at 4°C, stained with Coomassie blue and analyzed by phosphor-imaging. Counts corresponding to native actin in each lane were standardized to the Coomassie signal of the CCT band to account for any slight variations in gel loading.

DNaseI-Binding Assays

Triplicate 500 μg lysate samples were incubated with an excess (20 μl) of packed DNaseI-conjugated Affigel-10 beads for 3 hr at 4°C on a rotating wheel. DNase I beads were removed by centrifugation and the levels of actin remaining in the supernatant determined by western blotting. The actin antibody was the mouse monoclonal C4 from Seven Hills Bioreagents.

Hsp104-GFP Aggregation Retention Efficiency Assay

Cells expressing an Hsp104-GFP chromosomal fusion were grown to mid-log phase (OD_{600} ≈ 0.5) in YPD medium at 30°C (22°C for TS mutants) and then shifted to 42°C heat shock for 30 min. Cells were transferred back to 30°C for recovery and samples (2 ml aliquots) were taken in triplicate every 10 min. To analyze inheritance of protein aggregates during the subsequent budding event images were acquired using a Zeiss Axiovert 200 M fluorescence microscope. Budding events were marked manually in the bright-field channel first and then copied onto the GFP channel to avoid any possible bias on cell marking. The efficiency of segregation is expressed as percentage of mother cells capable of retaining all aggregates during cytokinesis. A BY4741 strain harbouring Hsp104-GFP was used as a wild-type control strain for the deletion mutants, and *his3*Δ Hsp104-GFP was a wild-type control for TS mutants. The *ura6-4* Hsp104-GFP strain was a control for TS mutants which did not show a genetic interaction with *SIR2* mutant. To calculate the retention efficiency of mother cells, between 300–600 budding events were counted for each strain.

Hsp104-GFP Aggregation Clearance Assay

Hsp104-GFP wild-type cells were grown to mid-log phase (OD_{600} = 0.5) in YPD at 30°C and then shifted to 38°C for 16 hr (aggregates will keep forming in the cell at this temperature). Samples were taken in triplicate and fixed, and images were taken randomly using a Zeiss fluorescent microscope. All clear budding events and single cells on every image were marked. A total of 300 budding events and single cells were counted for visible aggregates at each time point for each strain. The biomass increase was also measured at the same time. Aggregate clearance efficiency (ACE) was calculated as % buds able to clear themselves of all aggregates in 90–150 min after heat shock (38°C).

Nicotinamide and Resveratrol Treatment

Nicotinamide (final concentration of 5 mM) was added 10 min before heat shock treatment and directly after heat shock treatment. For the resveratrol assay, resveratrol (final concentration of 200 μM) was added to cultures at 10 min before heat shock. A corresponding amount of ethanol was added to the control.

Isolation of Old Cells

Old mother cells were obtained by magnetic sorting (Smeal et al., 1996). Exponentially growing cells were harvested, washed four times in ice-cold PBS, and labeled with 1 mg/ml Sulfo-NHS-LC Biotin (Pierce). The cells were allowed to grow overnight followed by incubation at 4°C for 2 hr with 250 μl streptavidin-conjugated paramagnetic beads (5 mg/ml Magnabind). Unlabeled cells were removed by magnetic sorting. The cells were then grown overnight in 100 ml YPD. The separation process was repeated twice and after the last separation 10 ml of cell-culture was centrifuged and resuspended in PBS.

Life-Span Analysis

Replicative life span was determined using a micromanipulator (Singer Instruments) and following the protocol as described (Kennedy et al., 1994). Experiments were performed independently at least twice for each strain, with 64 virgin cells per plate.

Time-Lapse Fluorescence Imaging

Cells were grown in YPD until mid-log phase (OD_{600} = 0.5) at 30°C. Aggregates were induced with heat shock at 42°C as explained previously, and then cells were recovered for 10 min at 30°C and 5 min at 23°C. Images were acquired every minute for 30–40 min. QuickTime movies were made from time-lapse images using GraphicsGale version 1.93.07.

Detection of Protein Interactions by In Situ Proximity Ligation Assay

Mid-log phase BY4741 and *hsp104*Δ strains were heat shocked (20 min) to induce Hsp104p expression. The rabbit anti-Hsp104 polyclonal antibody (MBL) and the mouse anti-actin (clone 4) monoclonal antibody (Seven Hills Bioreagents) were used to detect the interaction between Act1p and Hsp104p. Cells were harvested and pretreated based on standard immunofluoresence staining protocols with modifications. The PLA assay was performed as described previously (Soderberg et al., 2006), and the PLA signals were detected with Duolink PLA detection kit 563. Images were acquired using a Zeiss fluorescence microscope with bright-field (22

ms), Dapi (200 ms), and Cy3 (200 ms) channel. The signals in single cells were quantified by using Blobfinder software (Allalou and Wählby, 2009).

SUPPLEMENTAL REFERENCES

Allalou, A., and Wählby, C. (2009). BlobFinder, a tool for fluorescence microscopy image cytometry. Comput. Methods Programs Biomed. *94*, 58–65.

Boyle, E.I., Weng, S., Gollub, J., Jin, H., Botstein, D., Cherry, J.M., and Sherlock, G. (2004). GO:TermFinder–open source software for accessing Gene Ontology information and finding significantly enriched Gene Ontology terms associated with a list of genes. Bioinformatics *20*, 3710–3715.

Breitkreutz, B.-J., Stark, C., and Tyers, M. (2003). Osprey: a network visualization system. Genome Biol. *4*, R22.

Breitkreutz, B.J., Stark, C., Reguly, T., Boucher, L., Breitkreutz, A., Livstone, M., Oughtred, R., Lackner, D.H., Bahler, J., Wood, V., et al. (2008). The BioGRID Interaction Database: 2008 update. Nucleic Acids Res. *36*, D637–D640.

Ivy, J.M., Klar, A.J., and Hicks, J.B. (1986). Cloning and characterization of four *SIR* genes of *Saccharomyces cerevisiae.* Mol. Cell. Biol. *6*, 688–702.

Kennedy, B.K., Austriaco, N.R., Jr., and Guarente, L. (1994). Daughter cells of *Saccharomyces cerevisiae* from old mothers display a reduced life span. J. Cell Biol. *127*, 1985–1993.

Liou, A.K., and Willison, K.R. (1997). Elucidation of the subunit orientation in CCT (chaperonin containing TCP1) from the subunit composition of CCT micro-complexes. EMBO J. *16*, 4311–4316.

Rine, J., and Herskowitz, I. (1987). Four genes responsible for a position effect on expression from HML and HMR in *Saccharomyces cerevisiae.* Genetics *116*, 9–22.

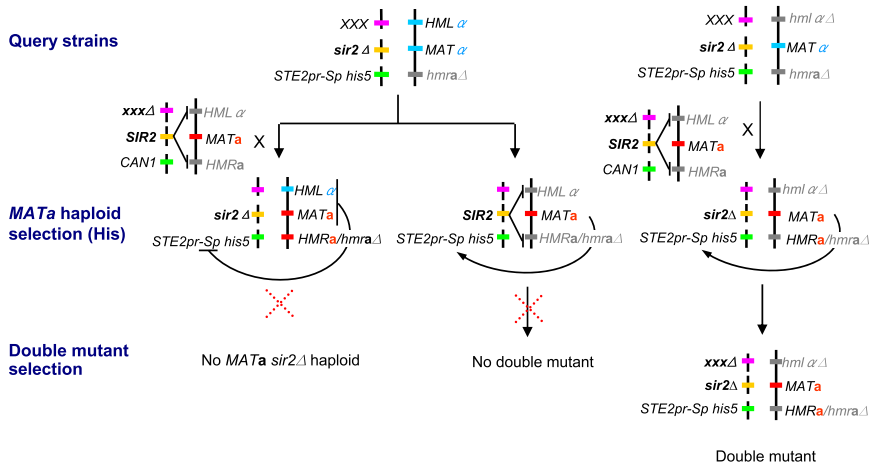

Figure S1. Construction of a *sir2*Δ Query Strain for SGA Analysis, Relates to Figure 1

The *sir2Δ* haploid strain is sterile due to loss of silencing at the silent mating type loci, *HML* and *HMR,* which result in coexpression of α and a mating types. To enable mating, the *HMR* locus was deleted in a *sir2*Δ *MAT*α query strain background. However, in the *MAT***a** meiotic progeny selection step, the *sir2*Δ *MAT***a** cell will inherit one copy of *HML* from the diploid, which will be co-expressed with the *MAT***a** gene. This will repress the SGA reporter (*can1*Δ*::STE2pr-Sp_his5*) and make it impossible to select for *MAT***a** haploids carrying a *SIR2* deletion. Therefore, deletion of the *HML* locus in the query strain is required for performing the *MAT***a** haploid selection step of the SGA screen. Colored mating type loci indicate that loci were expressed and gray ones indicate that the loci were silenced or deleted.

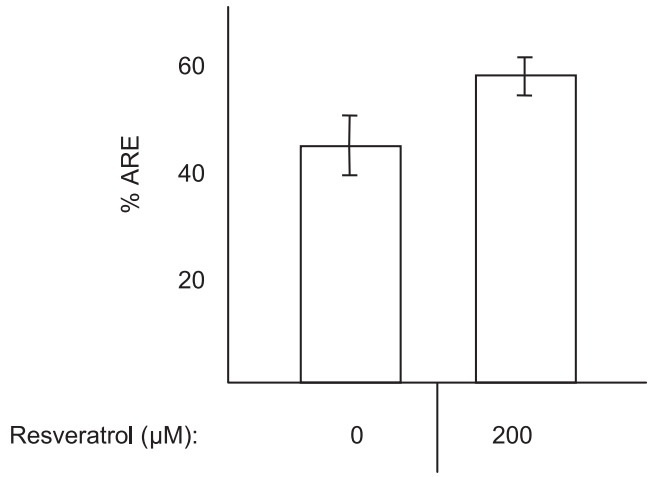

Figure S2. Addition of the Sir2p Activator Resveratrol to the Media before Heat Shock Enhances the Aggregation Retention Efficiency, Relates to Figure 4

Resveratrol was added to cultures 10 min prior to heat shock. The same amount of ethanol was added to the control. *y* axis shows the aggregation retention efficiency of untreated and 200 μM resveratrol-treated cells. Data are represented as mean ± SD.

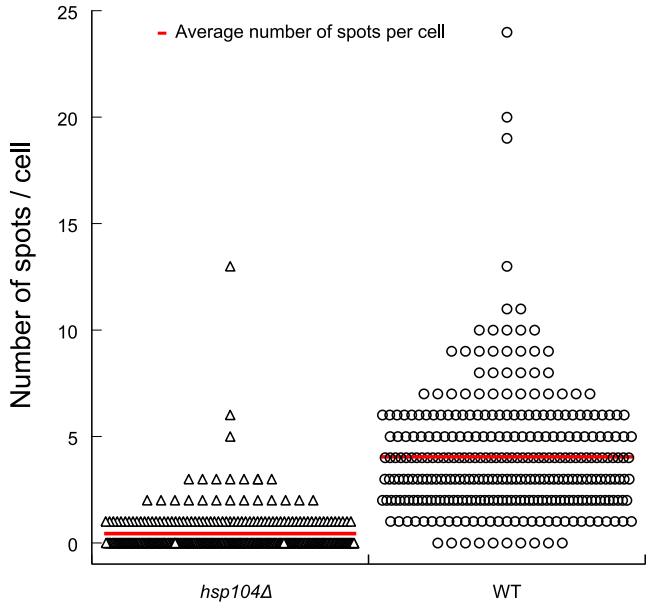

Figure S3. Quantification of Act1p and Hsp104p Interaction in Single Cells, Relates to Figure 5

y axis shows the number of PLA signals per cell as counted in 300 cells for either *hsp104*Δ or WT (By4741) cell cultures. The red horizontal lines indicate the average.